A Flavodiiron Protein and High Molecular Weight Rubredoxin from *Moorella thermoacetica* with Nitric Oxide Reductase Activity†

Radu Silaghi-Dumitrescu,‡ Eric D. Coulter,‡ Amaresh Das,§ Lars G. Ljungdahl,§ Guy N. L. Jameson,|| Boi Hanh Huynh,|| and Donald M. Kurtz, Jr.*,‡

Department of Chemistry and Center for Metalloenzyme Studies and Department of Biochemistry and Molecular Biology and Center for Biological Resource Recovery, University of Georgia, Athens, Georgia 30602, and Department of Physics, Emory University, Atlanta, Georgia 30322

Received November 27, 2002; Revised Manuscript Received January 20, 2003

ABSTRACT: A five-gene "oxidative stress protection" cluster has recently been described from the strictly anaerobic, acetogenic bacterium, *Moorella thermoacetica* [Das, A., et al. (2001) *J. Bacteriol. 183*, 1560−1567]. Within this cluster are two cotranscribed genes, *fprA* (for A-type flavoprotein) and *hrb* (for high molecular weight rubredoxin) whose encoded proteins have no known functions. Here we show that FprA and Hrb are expressed in *M. thermoacetica* under normal anaerobic growth conditions and report characterizations of the recombinant FprA and Hrb. FprA contains flavin mononucleotide (FMN) and a non-heme diiron site. Mössbauer spectroscopy shows that the irons of the diferric site are antiferromagnetically coupled, implying a single-atom, presumably solvent, bridge between the irons. Hrb contains FMN and a rubredoxin-like [Fe(SCys)$_4$] site. NADH does not directly reduce either the FMN or the diiron site in FprA, whereas Hrb functions as an efficient NADH:FprA oxidoreductase. Substitution of zinc for iron in Hrb completely abolished this activity. The observation that homologues of FprA from other organisms show O_2 and/or anaerobic NO consumption activity prompted an examination of these activities for *M. thermoacetica* FprA. The Hrb/FprA combination does indeed have both NADH:O_2 and NADH:NO oxidoreductase activities. The NO reductase activity, however, was significantly more efficient due to a lower K_m for NO (4 μM) and to progressive and irreversible inactivation of FprA during O_2 reductase turnover but retention of activity during NO reductase turnover. Substitution of zinc for iron in FprA completely abolished these reductase activities. The stoichiometry of 1 mol of NADH oxidized:2 mol of NO consumed implies reduction to N_2O. Fits of an appropriate rate law to the kinetics data are consistent with a mechanism in which 2NO's react at each FprA active site in the committed step. Expression of FprA in an *Escherichia coli* strain deficient in NO reductase restored the anaerobic growth phenotype of cultures exposed to otherwise toxic levels of exogenous NO. The accumulated results indicate that Hrb/FprA is fully capable of functioning in nitrosative stress protection in *M. thermoacetica*.

Moorella thermoacetica [formerly, *Clostridium thermoaceticum* (*1*)], originally isolated from horse manure, is the most thoroughly studied member of the acetogens, a group of Gram-positive, obligately anaerobic bacteria found in virtually any anoxic environment (*2*, *3*). For many years it was believed that *M. thermoacetica* could use only carbon dioxide as terminal electron acceptor and that the metabolism of carbon dioxide into acetate via the Wood−Ljungdahl pathway was obligatory for growth and survival of this bacterium (*4*). Recent studies indicate, however, that, when given a choice, *M. thermoacetica* will use nitrate preferentially over carbon dioxide as the electron acceptor via an apparently dissimilatory pathway with a variety of small carbon compounds as electron donors (*5*−*7*).

In recent years, the realization has emerged that nondenitrifying bacteria also have complex systems for metabolizing the lower oxides of nitrogen. Included in this metabolism is detoxification of nitric oxide generated endogenously, as a consequence of nitrate/nitrite reduction, and/or exogenously, either from other bacteria or as a host response to infection or colonization (*8*−*10*). Anaerobic bacteria, presumably including acetogens, must, thus, cope with "nitrosative" stress in addition to "oxidative" stress due to transient exposure to dioxygen (*11*).

A five-gene "oxidative stress protection" cluster in *M. thermoacetica* has recently been described (*12*). Within this cluster are two cotranscribed genes, *fprA* (for A-type flavoprotein) and *hrb* (for high molecular weight rubredoxin) whose encoded proteins have no known functions and for which only preliminary characterizations were reported. The gene, *hrb*, encodes a unique 229-residue protein, Hrb, the amino acid sequence of which can be divided into two domains, based on homologies to other proteins. The

† This work was supported by Grants GM40388 (D.M.K.) and GM 58778 (B.H.H.) from the National Institutes of Health and Grant DE-FG02-93ER20127 from the Department of Energy (L.G.L.).

* To whom correspondence should be addressed at the Department of Chemistry, University of Georgia. Phone: 706-542-2016. Fax: 706-542-9454. E-mail: kurtz@chem.uga.edu.

‡ Department of Chemistry and Center for Metalloenzyme Studies, University of Georgia.

§ Department of Biochemistry and Molecular Biology and Center for Biological Resource Recovery, University of Georgia.

|| Department of Physics, Emory University.

10.1021/bi027253k CCC: $25.00
Published on Web 02/20/2003

N-terminal domain sequence is homologous to a flavoprotein with ferric reductase activity from the sulfate-reducing archaeon, *Archaeoglobus fulgidus* (*13*, *14*), and the C-terminal domain sequence is homologous to that of the non-heme iron, electron transport protein, rubredoxin (*12*). The amino acid sequence of the 398-residue protein, FprA, encoded by the *M. thermoacetica fprA*, is homologous to that of a flavoprotein referred to as rubredoxin:oxygen oxidoreductase (ROO) from the anaerobic, sulfate-reducing bacterium, *Desulfovibrio gigas*. The heme-contaminated *D. gigas* ROO, together with rubredoxin and a rubredoxin reductase, was shown to have dioxygen reductase activity (*15*) and was proposed to catalyze the four-electron reduction of dioxygen to water by NADH (*16*). The subsequently determined X-ray crystal structure of *D. gigas* ROO showed a homodimer with each subunit folded into two distinct domains. The C-terminal FMN binding domain is structurally (and sequentially) homologous to flavodoxins. The N-terminal domain was found to be structurally homologous to dimetal β-lactamases and to contain a non-heme diiron site. No heme or potential heme binding sites were found in the ROO crystal structure, and the reduction of dioxygen was, therefore, proposed to occur at the non-heme diiron site (*17*). The head-to-tail orientation of the subunits in the ROO homodimer brings the FMN from one subunit in close proximity to the diiron site of the other subunit, which presumably facilitates electron transfer. The *M. thermoacetica* FprA amino acid sequence conserves all of the iron-ligating residues found in *D. gigas* ROO as well as the C-terminal flavodoxin-like domain. These two proteins are members of a recently recognized family of apparent flavodiiron proteins which, based on genome sequences, are widely distributed among anaerobic archaea and bacteria (*18*−*20*), with homologues also present in some facultative anaerobes, such as *Escherichia coli*.

In fact, clear genetic evidence was recently reported showing that inducible nitric oxide consumption by anaerobically growing *E. coli* is due to its FprA homologue, named flavorubredoxin (FlRd)[1] because it contains an additional rubredoxin-like domain (*21*−*23*). Disruption of the FlRd gene resulted in an *E. coli* strain whose growth was inhibited relative to the wild type upon anaerobic exposure to ≤ 1 μM nitric oxide in minimal media (*21*) or to 100 μM levels of nitroprusside in rich media (*23*). *E. coli* FlRd was, therefore, proposed to be the terminal component of a nitric oxide reductase and to utilize its putative non-heme diiron site to catalyze reduction of nitric oxide to nitrous oxide (*21*). The purified recombinant FlRd and its associated NADH:FlRd oxidoreductase were initially shown to have dioxygen reductase activity (*24*) but, more recently, to have NO reductase activity (*25*). Here we present our characterizations of *M. thermoacetica* FprA and Hrb and demonstrate the NO reductase functionality of FprA both in vitro and in vivo.

[1] Abbreviations: LB, Luria−Bertani medium; EDTA, ethylenediaminetetraacetic acid; MOPS, 3-(*N*-morpholino)propanesulfonic acid; IPTG, isopropyl β-D-thiogalactoside; DEA NONOate, diethylammonium (*Z*)-1-(*N*,*N*-diethylamino)diazen-1-ium 1,2-diolate; SDS−PAGE, sodium dodecyl sulfate−polyacrylamide gel electrophoresis; SHE, standard hydrogen electrode; MES, 1-(*N*-morpholino)ethanesulfonic acid; NOR, nitric oxide reductase; FlRd, flavorubredoxin; FMN_{ox}, oxidized FMN; FMN_{sq}, one-electron-reduced FMN (semiquinone), FMN_{red}, two-electron-reduced FMN (hydroquinone).

MATERIALS AND METHODS

Reagents and General Procedures. *M. thermoacetica* (ATCC 39073) was grown at 58 °C in the presence of 100 mM methanol under 100% CO_2 in either the presence or absence of reducing agents (Na_2S, 0.25 g/L; cysteine hydrochloride, 0.25 g/L) (*5*, *11*). *M. thermoacetica* cell extracts were prepared by breakage of the cells in a French press (*26*). All solutions were prepared in deionized water. Glucose oxidase from *Aspergillus niger*, β-D-(+)glucose, catalase from bovine liver, horse heart cytochrome *c*, NADH, and NADPH (Sigma Chemical Co.) and protein molecular weight standards (Bio-Rad, Inc.) were used without further purification. Redox dyes were purchased from Aldrich or Sigma. Molecular biology manipulations followed standard protocols (*27*). DNA restriction and ligating enzymes were obtained from New England Biolabs, Inc. Stock solutions (25 mM) of DEA NONOate (Cayman Chemicals, Inc.) were prepared in 0.01 M NaOH. DEA NONOate is stable at high pH but decomposes to release NO gas (1.5 mol of NO/1 mol of DEA NONOate) when added to assay mixtures at pH ~7. Where indicated, solutions were made anaerobic by repetitive vacuum/argon or N_2 gas exchange or extensive purging with argon or N_2 gas. Gaseous nitric oxide (98.5%) was purchased from Aldrich. The NO was purified by bubbling through 100 mL of a 10% KOH solution. The purified NO gas was used to prepare saturated NO solutions (~1.8 mM) by bubbling the gas through anaerobic deionized water for 15 min. Protein purity was judged by SDS−PAGE (15% polyacrylamide gels) and Coomassie blue staining (*28*). Western blotting followed a standard procedure (*29*). Antibodies against purified recombinant *M. thermoacetica* FprA and Hrb were raised in rabbits at the Animal Care and Use Facility at the University of Georgia and purified from serum by a standard procedure (*30*).

FprA Expression and Purification. Fifty milliliter cultures of *E. coli* BL21-Gold (DE3) (Stratagene, Inc.) transformed with pFprA [a pET-21(b+) (Novagen, Inc.) derivative containing the *M. thermoacetica fprA* (*12*)] were grown with shaking at 37 °C in M-9 minimal media containing 100 μg of ampicillin/mL. After overnight growth the 50 mL cultures were used to inoculate 1 L volumes of the same media. The 1 L cultures were grown with shaking at 37 °C to an OD (600 nm) of ~0.6, at which point isopropyl β-D-thiogalactoside (100 mg/L) was added to induce expression of FprA. The cultures were supplemented at the time of induction with 10 mg of ferrous sulfate/L or 10 mg of zinc sulfate/L for zinc-substituted proteins. After a further 4 h incubation/shaking at 37 °C, the cells were harvested by centrifugation. The recombinant FprA was typically purified from cells harvested from twelve 1 L cultures. Unless otherwise specified, the buffer used throughout protein purification was 50 mM MOPS, pH 7.3. After a −80 °C freeze−thaw cycle the harvested cells were resuspended in 10 mL of buffer/L of culture and lysed by sonication (*31*). The supernatant was loaded onto a 1.6 × 2.5 HiTrap anion-exchange column [Amersham Pharmacia BioTek(APBT)] equilibrated with buffer and eluted at a flow rate of 3 mL/min using a gradient of NaCl. FprA eluted as a yellow-orange fraction at ~200 mM NaCl. Fractions exhibiting similar UV−vis absorption spectra were pooled, concentrated to ~2 mL/4 L of culture, and loaded onto a HiPrep 16/60 Sephacryl S-100 column

(APBT) equilibrated with buffer + 250 mM NaCl and eluted at 0.5 mL/min. Yellow-orange eluting fractions exhibiting similar UV−vis absorption spectra were pooled and desalted by repeated concentrations/dilutions. The desalted protein solution was concentrated to ~5 mL and loaded onto a 1.6 × 2.5 HiTrap anion-exchange column equilibrated with buffer and eluted at a flow rate of 3 mL/min using a gradient of NaCl. The FprA eluted as a single yellow-orange band. Yields of the purified recombinant FprA were typically ~4 mg/L of *E. coli* culture. An analogous protocol was used to purify recombinant FprA in similar yields using the plasmid pFprA-pCYB1 in place of pFprA. The plasmid, pFprA-pCYB1, was constructed by inserting the PCR-amplified *M. thermoacetica fprA* (*12*) into the *Nde*I/*Eco*RI restriction sites of pCYB1 (New England Biolabs, Inc.).

His-Tagged FprA Expression and Purification. To obtain a recombinant His-tagged FprA, the stop codon in pFprA was removed using the QuickChange mutagenesis kit (Stratagene, Inc.) with the primers 5′-CGCATAGCCGATCTGAATTCGAGCTC-3′ (forward) and 5′-GAGCTCGAATTCAGATCGGCTATGCG-3′ (reverse) following procedures described in the product manual. The His-tagged FprA was expressed in *E. coli* strain BL21 Gold (DE3) using a procedure identical to that described for the non-His-tagged FprA, except that the cultures were supplemented with 1 mg of ^{57}Fe/L [iron powder, 95 atom % ^{57}Fe enriched (Advanced Materials Technologies, Ltd.), dissolved in a 2-fold molar excess of H_2SO_4] when the protein was to be used for Mössbauer spectroscopy. Cells harvested from 5 L of culture were subjected to one freeze−thaw cycle, then resuspended in 50 mL of 50 mM phosphate, pH 7, containing 300 mM NaCl (high-salt buffer), and loaded onto a cobalt-containing Talon Cell-thru column (Clontech Laboratories, Inc.) equilibrated in the high-salt buffer. His-tagged FprA eluted as pure protein (as judged by SDS−PAGE) upon washing the column with the high-salt buffer containing 150 mM imidazole. The eluted protein was then transferred into 50 mM MOPS, pH 7.3, by repeated dilutions and concentrations in an Amicon cell (YM10 membrane). His-tagged FprA yields were typically ~9 mg/L of *E. coli* culture.

Hrb Expression and Purification. The full-length *hrb* was PCR-amplified from *M. thermoacetica* genomic DNA (*12*) using the appropriate forward and reverse oligonucleotide primers with sequences duplicating the 5′ and 3′ ends, respectively, of the gene. The primers also contained unique restriction sites at their 5′ ends, *Nde*I for the forward primer and *Eco*RI for the reverse primer. The purified PCR products (QIAquick PCR purification kit, Qiagen, Inc.) were digested with *Nde*I and *Eco*RI and ligated into the corresponding restriction sites of pCYB1 (New England Biolabs, Inc.), yielding pHrb. Recombinant Hrb was expressed from *E. coli* BL21 Gold (DE3) that had been transformed with pHrb and was purified by procedures identical to those described for FprA with the following exceptions. Low-light conditions and 4 °C buffers were used because prolonged exposures of Hrb to normal room light and temperature were found to promote protein degradation, and the final HiTrap anion-exchange step was not used because, based on SDS−PAGE, the preceding gel filtration step yielded a pure protein. Hrb yields were typically ~10 mg/L of *E. coli* culture.

Analytical Methods. Protein concentrations were determined using the Bio-Rad protein assay (Bio-Rad, Hercules, CA) with bovine serum albumin as the standard. Metal contents of Hrb and FprA were determined by inductively coupled plasma-atomic emission analysis at the University of Georgia Chemical Analysis Facility. Flavin was identified and quantitated as described previously (*12*). Molar absorptivities (listed in Table 1) were determined from the protein quantitations, and these values were subsequently used to calculate all protein concentrations from measured absorbances.

Table 1: Properties of Purified Recombinant FprA and Hrb from *M. thermoacetica*

	FprA	Hrb
molecular mass, kDa		
calcd from sequence	44.3	24.9
from SDS−PAGE	45	23
from gel filtration	91	45
cofactor content, mol/mol of homodimer		
iron[a] (zinc)[b]	3.8 ± 0.5 (4)[b]	2.0 ± 0.1 (2)[b]
FMN	1.7 ± 0.1	1.6 ± 0.3
optical absorption spectra, nm	278	278
(ϵ, mM homodimer^{-1} cm^{-1})[c]	350	350
	374, sh	377, sh
	450 (24)	450, 474 (34)
		565, sh
reduction potentials (mV vs SHE)[d]		
FMN_{ox}/FMN_{sq}	−117	−121
FMN_{sq}/FMN_{red}	−220	−121
$[Fe^{III/II}(SCys)_4]$		−30

[a] For proteins grown in minimal medium supplemented with iron. [b] Parenthetical values are zinc content of proteins expressed from *E. coli* cultured in M9 minimal medium supplemented with $ZnSO_4$ in place of $FeSO_4$. [c] In 50 mM MOPS, pH 7.3. [d] In 50 mM MOPS, pH 7.0. The estimated error range for each listed potential is ±10 mV. Nernst plots are included as Supporting Information.

Redox Potentials. A spectrophotometric, dye-mediated, electrochemical titration method was used similar to that described for *E. coli* FlRd (*24*). All measurements were conducted at room temperature (~23 °C) in 50 mM MOPS, pH 7.0. Further experimental details are provided as Supporting Information.

NADH:O_2 and NADH:NO Oxidoreductase Assays. FprA and Hrb concentrations and buffers used in these assays are listed in the figure legends. All assays were performed at pH 7.0 and room temperature (~23 °C). Hrb/FprA-dependent NADH oxidase (O_2-consumption) assays were monitored in air-saturated buffer either as decreasing absorbance at 340 nm due to O_2-dependent NADH oxidation or as O_2 consumption rates, measured polarographically using a Yellow Springs Instruments Model 5300 biological oxygen monitor equipped with a Clark-type oxygen electrode. NO reductase (NO consumption) activities were assayed anaerobically by monitoring the decrease in absorbance at 340 nm due to NO-dependent NADH consumption. NO, from either a stock DEA NONOate or an NO-saturated aqueous solution, was introduced into the anaerobic assay mixture via a Hamilton gastight syringe. Alternatively, the NADH-dependent NO reductase activity was followed under anaerobic conditions by measuring the decrease in NO concentration with time using a Clark-type NO-sensitive electrode [ISO-NOP, 2 mm diameter, World Precision Instruments, Inc. (WPI)]. NO electrode measurements were performed on magnetically stirred solutions inside a 2 mL anaerobic glass chamber (WPI), the headspace of which was continuously purged with

nitrogen gas through a needle inserted into one of the two narrow ports of the chamber. Reagents were introduced through the second port via Hamilton gastight syringes. The assay solutions contained the indicated initial concentrations of NO, injected from a saturated aqueous solution, and after a short background trace was measured, the reaction was initiated by addition of FprA. The small background NO consumption rate, amounting to a few percent of that after addition of FprA, was subtracted to obtain the FprA-dependent NO consumption rates. For both methods of measuring NO consumption, anaerobicity of the assay solutions was ensured by inclusion of a dioxygen-scrubbing system consisting of 5 mM glucose, 8 units/mL glucose oxidase, and 150 units/mL catalase.

Spectroscopy. Ultraviolet−visible absorption spectra were obtained in 1 cm path length quartz cuvettes on a Shimadzu UV-2401PC scanning spectrophotometer. EPR spectra were recorded on a Bruker ESP-300E spectrometer equipped with an ER-4116 dual-mode cavity and an Oxford Instruments ESR-9 flow cryostat. Mössbauer spectra were recorded on either a weak-field spectrometer with a Janis 8DT variable temperature cryostat or a strong-field spectrometer furnished with a CNDT/SC Super-Varitemp cryostat encasing an 8T superconducting magnet. Both spectrometers operate in a constant acceleration mode in transmission geometry. The zero velocity of the spectra refers to the centroid of a room temperature spectrum of metallic iron foil. The Mössbauer spectra were analyzed using the WMOSS program (WEB Research Co., Edina, MN) based on a spin Hamiltonian formalism conventionally used for Mössbauer analysis. Mössbauer spectroscopy employed as-isolated His-tagged ^{57}Fe-enriched FprA (0.5 mM homodimer in 50 mM MOPS, pH 7.3).

FprA Complementation of E. coli Growth Sensitivity to NO. *E. coli* strain AG300, containing a disrupted FlRd gene (*norV*), was kindly provided by Paul R. Gardner (*21*). The anaerobic growth medium contained 60 mM K_2HPO_4, 33 mM KH_2PO_4, 7.6 mM $(NH_4)_2SO_4$, 1.7 mM sodium citrate, 1 mM $MgSO_4$, 10 μM $MnCl_2$, 10 μM thiamin hydrochloride, 2% potassium gluconate, 0.25% casamino acids, ampicillin (0.1 g/L), and chloramphenicol (0.1 g/L). Anaerobic cultures were grown without shaking at 37 °C under N_2 gas. Ten milliliter cultures of *E. coli* AG300 transformed with either pCYB1 or pFprA-pCYB1 were grown overnight aerobically at 37 °C in LB medium containing ampicillin (0.1 g/L) and chloramphenicol (0.1 g/L). One-half milliliter of the aerobic cultures was inoculated into 25 mL of anaerobic culture medium in 50 mL sealed flasks. The anaerobic cultures were grown at 37 °C until OD (550 nm) ~0.6, at which point 0.5 mL aliquots were used to inoculate fresh 25 mL batches of anaerobic culture medium. This cycle was repeated a third time. At OD ~0.6, 1 mL aliquots of the third subcultures were used to inoculate 150 mL flasks, each containing 100 mL of anaerobic culture medium. Results reported below were obtained with these 100 mL cultures. IPTG (0.05 mg/L) was added to each 100 mL culture at OD (550 nm) ~0.1. Where required, aliquots of either an NO-saturated aqueous solution or 25 mM DEA NONOate were added to the 100 mL cultures 60 min after IPTG addition. Initial concentrations of added NO are given in the figure legends.

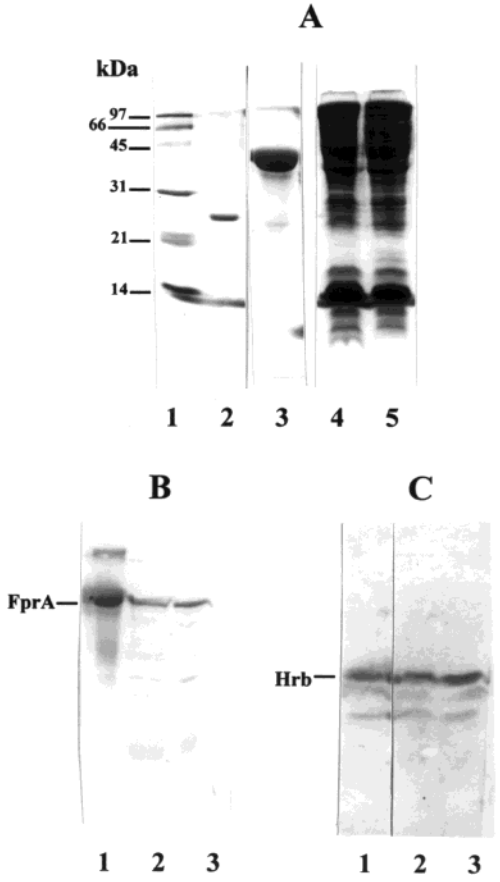

FIGURE 1: SDS−PAGE (A) and Western blots (B and C) of whole cell extracts of *M. thermoacetica* probed with antibodies raised against recombinant *M. thermoacetica* FprA (B) or Hrb (C). Panel A: lane 1, protein standards; lane 2, purified Hrb (2 μg); lane 3, purified FprA (2 μg); lanes 4 and 5, *M. thermoacetica* cell extracts (30 μg) grown in either the absence (lane 4) or presence (lane 5) of reducing agents (cf. Materials and Methods). (A strong band of molar mass ~14 kDa in lanes 4 and 5 corresponds to lysozyme used to lyse the cells.) Panels B and C: lanes 1 contain purified recombinant FprA (panel B) or Hrb (panel C); lanes 2 and 3 are the same as lanes 4 and 5, respectively, of panel A.

RESULTS AND DISCUSSION

Expression of FprA and Hrb in M. thermoacetica. Our original investigation of *fprA* and *hrb* demonstrated their transcriptions but not their translations in *M. thermoacetica*. We, therefore, raised antibodies against the purified recombinant FprA and Hrb and probed *M. thermoacetica* cell extracts by immunoblotting. The Western blots in Figure 1 show that FprA and Hrb are produced in *M. thermoacetica* grown anaerobically with methanol/CO_2 as electron donor/acceptor, i.e., via the Wood−Ljungdahl pathway. No significant differences in the levels of either FprA or Hrb were noted in cells grown in the presence vs absence of added reducing agents, the latter growth conditions constituting a mild oxidative stress.[2]

Properties of Recombinant M. thermoacetica FprA. The originally reported expression and isolation of recombinant *M. thermoacetica* FprA from *E. coli* cultured in LB media yielded a protein with substoichiometric amounts of cofactors

[2] A lag phase in growth was noted in the absence of added reducing agents similar to that reported when *M. thermoacetica* cultures were exposed to small amounts of O_2 (*11*).

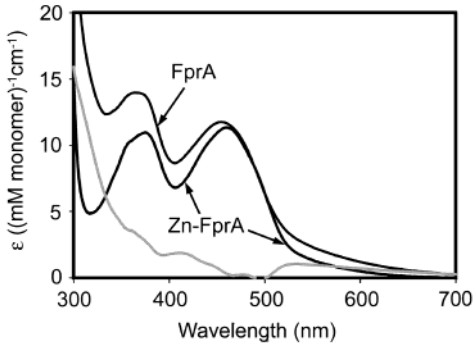

FIGURE 2: UV−vis absorption spectra of recombinant as-isolated *M. thermoacetica* FprA, Zn−FprA, and the difference spectrum: FrpA minus Zn−FprA (gray trace). Buffer is 50 mM MOPS, pH 7.3. Spectra were obtained under an aerobic atmosphere.

relative to that expected for full occupancy of its metal and flavin binding domains (*12*). As can be seen from the analytical data in Table 1, however, when *E. coli* harboring the *fprA* expression plasmid was grown in minimal medium supplemented with ferrous sulfate at the time of induction of FprA expression, the isolated and purified protein reproducibly contained 1.9 irons per monomer. This stoichiometry is close to the 2 expected for full occupancy of the dimetal site. Similarly, the 0.8−0.9 FMN/FprA monomer indicates nearly full occupancy of the single flavin binding site expected in each subunit. The recombinant FprA was isolated as a stable homodimer (cf. Table 1). When the recombinant FprA was expressed from *E. coli* cultures grown in minimal medium supplemented with zinc sulfate, the isolated protein had the same FMN content as for FprA isolated from iron-supplemented cultures but contained approximately 2 zincs per monomer and very little iron. We refer to protein prepared in this latter fashion as Zn−FprA. The optical absorption spectra of the as-isolated, recombinant *M. thermoacetica* FprA and Zn−FprA, shown in Figure 2, are dominated by FMN. The difference absorption spectrum, FprA minus Zn−FprA, is presumably due to the diferric site and/or the proximal FMN site that is perturbed by the Zn^{2+}-for-Fe^{3+} substitution. This latter possibility precludes firm conclusions about the diiron site structure or oxidation state from the FprA minus Zn−FprA difference UV−vis absorption spectrum. We, therefore, probed the iron environment in FprA with ^{57}Fe Mössbauer spectroscopy.

The optical absorption spectrum, cofactor content, and catalytic activity (see below) of the His-tagged FprA were identical to those of the non-His-tagged protein. ^{57}Fe Mössbauer spectra of the as-isolated, His-tagged FprA enriched with ^{57}Fe, shown in Figure 3, can be fit to two quadrupole doublets having the same isomer shift but different quadrupole splittings and asymmetry parameters (listed in the figure legend) and assuming diamagnetism. The isomer shift is typical of high-spin ferric iron, and the two quadrupole doublets suggest two different iron environments. The fact that the high-field Mössbauer spectrum (Figure 3B) can be well fit with the assumption of diamagnetism proves that the two ferric irons are antiferromagnetically coupled with a diamagnetic ground state. Consistent with this conclusion, the EPR spectrum of the as-isolated FprA obtained at 5 K (not shown) shows only a weak $g = 4.3$ resonance, indicative of adventitiously bound ferric iron, plus a narrow symmetrical resonance at $g = 2.005$, due to an

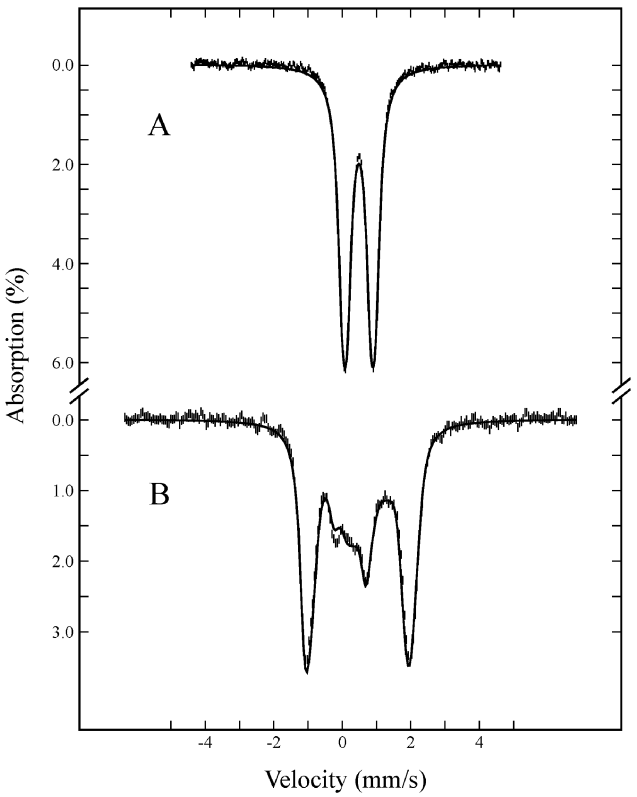

FIGURE 3: Mössbauer spectra of ^{57}Fe-enriched His-tagged as-isolated *M. thermoacetica* FprA (0.5 mM homodimer in 50 mM MOPS, pH 7.3) recorded at 4.2 K in magnetic fields of 50 mT (A) and 8 T (B) applied parallel to the γ-ray beam. The solid lines overlaying the experimental spectra (hatched marks) are least-squares fits to the data using two equal-intensity quadrupole doublets with $\delta_1 = \delta_2 = 0.49 \pm 0.02$ mm/s, $\Delta E_{Q1} = -0.69 \pm 0.03$ mm/s, $\Delta E_{Q2} = 0.97 \pm 0.03$ mm/s, $\eta_1 = 0.8$, and $\eta_2 = 0.0$ and assuming diamagnetism. The fitted line width for both quadrupole doublets was 0.33 mm/s.

organic free radical, presumably a small portion of FMN semiquinone.

Comparisons with carboxylato-bridged, non-heme diiron synthetic complexes and diiron proteins show that antiferromagnetic coupling in diferric sites is invariably associated with a single atom bridge (*32*). Since there is no evidence for acid-labile sulfide in FprA, the most obvious candidate for a single atom bridge is solvent. In fact, the X-ray crystal structure of *D. gigas* ROO showed an apparent solvent bridge between the two irons, which were separated by 3.4 Å (*17*). The two different iron environments of *M. thermoacetica* FprA revealed by the Mössbauer spectra are consistent with the asymmetric coordination sphere of the ROO diiron site. Redox potentials for the two sequential one-electron redox processes of the FMN cofactor in FprA are listed in Table 1. The average of these two potentials is similar to that reported for the FMN in *E. coli* FlRd [−160 mV (*24*)], but the FMN_{ox}/FMN_{sq} (−117 mV) and FMN_{sq}/FMN_{red} (−220 mV) potentials are somewhat more separated from each other in FprA (cf. Nernst plots in Figure 1S of Supporting Information).

Properties of Recombinant M. thermoacetica Hrb. When expressed and purified as described in Materials and Methods, a soluble recombinant Hrb was obtained which reproducibly contained 1 iron per subunit (cf. Table 1). This stoichiometry is consistent with the single rubredoxin-like

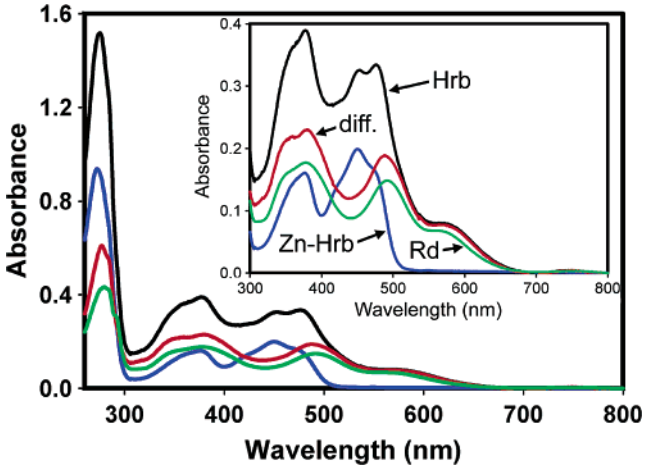

FIGURE 4: UV−vis absorption spectra (inset expanded by a factor of ~4) of as-isolated Hrb (20 μM monomer, black trace) and as-isolated Zn−Hrb (20 μM, blue trace) in aerobic 25 mM MOPS, pH 7.3. The difference spectrum of Hrb minus Zn−Hrb (red trace, labeled diff.) and *P. furiosus* rubredoxin (green trace, labeled Rd).

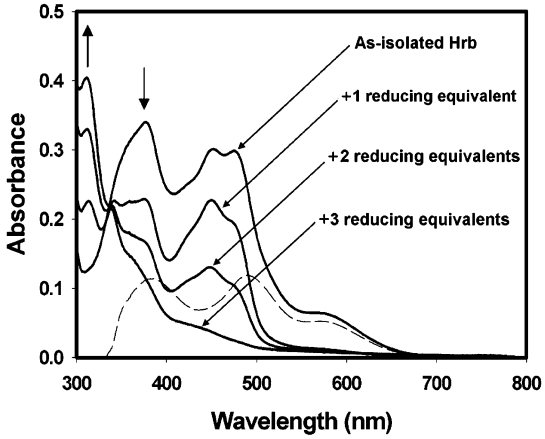

FIGURE 5: UV−vis absorption spectral changes upon anaerobic titration of *M. thermoacetica* Hrb (16 μM monomer) with NADH in 25 mM MOPS, pH 7.3. Arrows indicate the direction of absorbance changes with increasing NADH. The difference spectrum of as-isolated Hrb minus "+1 reducing equivalents added" is shown as a dashed trace.

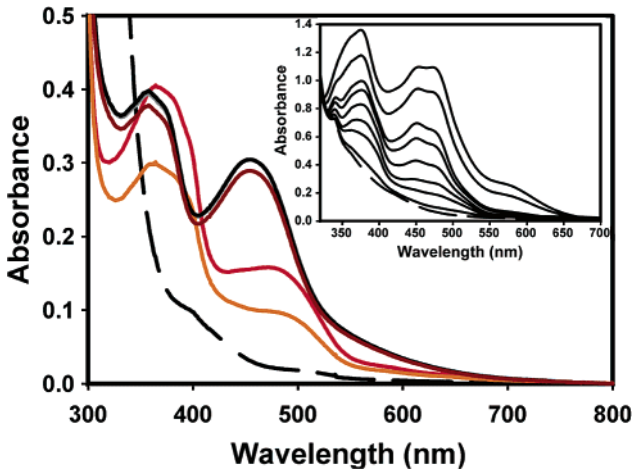

FIGURE 6: UV−vis absorption spectra obtained upon titration of *M. thermoacetica* FprA (20 μM in monomer) and catalytic Hrb (0.5 μM) with NADH in anaerobic 50 mM MOPS, pH 7.3. Black trace: as-isolated, no NADH. Maroon trace: after addition of 2 reducing equivalents of NADH per FprA monomer. Red trace: after addition of 3 reducing equivalents. Orange trace: 20 min after addition of 4 reducing equivalents. Dashed trace: fully reduced FprA, using a large excess of sodium dithionite. The inset shows monotonically decreasing UV−vis absorption during titration of equimolar FprA:Hrb (39 μM monomer, each) with NADH in anaerobic 50 mM phosphate, pH 7. Top trace: no NADH added. The remaining seven traces were recorded immediately after each of seven sequential additions of 1 reducing equivalent per monomer of NADH. Dashed trace: spectrum taken 5 min after addition of the seventh reducing equivalent (no further spectral changes were observed at longer incubation times).

domain in the deduced Hrb amino acid sequence (*12*). The recombinant Hrb was isolated as a homodimer. The flavin in recombinant Hrb was identified as FMN, which varied between 1.3 and 1.9 FMN per homodimer. A stoichiometry of 2 FMN/homodimer would be expected for full occupancy of the N-terminal ferric reductase-like domain of Hrb. Incomplete occupancy of the flavin binding sites was also noted in the *A. fulgidus* ferric reductase; only 1 FMN per homodimer was found in the X-ray crystal structure after in vitro reconstitution (*33*). Using the same method as for Zn−FprA, a recombinant zinc-substituted Hrb (Zn−Hrb) was isolated, containing FMN, approximately 1 Zn/monomer, and very little iron (cf. Table 1).[3]

The UV−vis absorption spectra of as-isolated recombinant Hrb and the corresponding Zn−Hrb are shown in Figure 4, and spectral data are listed in Table 1. Also shown in Figure 4 is the difference spectrum, Hrb minus Zn−Hrb, which closely resembles that of oxidized rubredoxin. The optical absorption spectrum of as-isolated Hrb is, thus, the sum of FMN and rubredoxin-like [$Fe^{III}(SCys)_4$] absorptions, as predicted from amino acid sequence homologies (*12*). The as-isolated Hrb also shows both an X-band EPR spectrum at 4 K (included as Figure 2S in Supporting Information) with *g* values at 4.35 and 9.65 and a reduction potential of the [$Fe(SCys)_4$] site(−30 mV) that are within the ranges of those reported for rubredoxins (*34*, *35*).

UV−vis absorption spectra obtained during an anaerobic titration of Hrb with NADH are shown in Figure 5. The spectral changes indicate that NADH can reduce both cofactors of Hrb, but the difference spectrum shows that the absorption features of the oxidized (ferric) [$Fe(SCys)_4$] site disappear essentially completely after the first reducing equivalent of NADH is added. This first reducing equivalent, thus, ends up in the [$Fe(SCys)_4$] site, as expected from its more positive reduction potential relative to that of the FMN cofactor (cf. Table 1). The semiquinone of FMN (i.e., the one-electron-reduced form), which is either red (anionic) or blue (neutral) depending on protonation state (*20*), did not appear to accumulate during either the NADH or electrochemical titrations (cf. Nernst plot in Figure 3S of Supporting Information) of Hrb. The absorption features appearing at ~310 and 330 nm upon reduction of Hrb are characteristic of the reduced, i.e., ferrous [$Fe(SCys)_4$] site (*36*). Since NADH is not known to directly reduce [$Fe^{III}(SCys)_4$] sites, these results imply that the electron flow is NADH → Hrb−FMN → Hrb−[$Fe(SCys)_4$].

[3] As-isolated Hrb in buffered solutions was prone to apparent autoproteolysis over the course of several hours at room temperature, giving rise to two fragments corresponding in size to the ferric reductase-like and rubredoxin-like domains. This fragmentation of Hrb coincided with progressive loss of its NADH:FprA oxidoreductase activity. We, therefore, routinely handled thawed Hrb solutions for only short periods and kept the solutions on ice or at 4 °C.

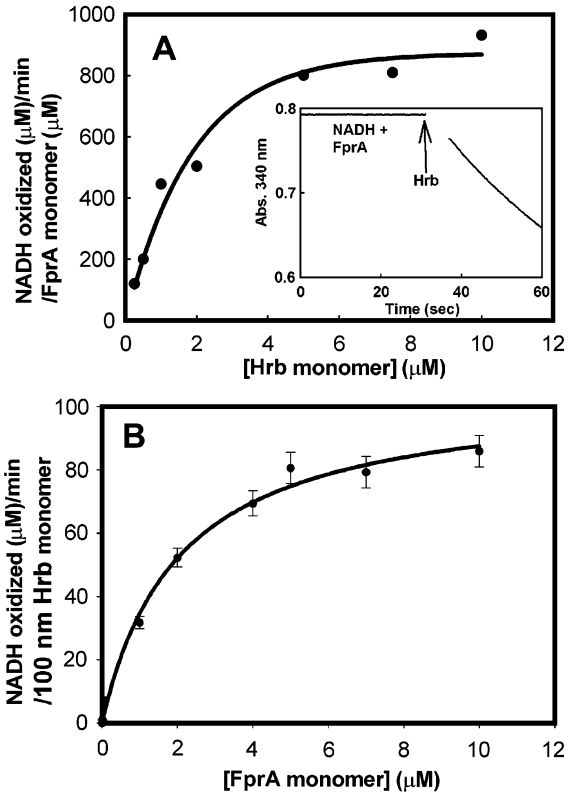

FIGURE 7: Concentration dependences of NADH:O_2 oxidoreductase activity of *M. thermoacetica* FprA/Hrb. (A) Plot of activity vs Hrb concentration. Conditions: 50 nM FprA homodimer, 200 μM NADH, and the indicated concentrations of Hrb in air-saturated 50 mM MOPS, pH 7.0 at 25 °C. Inset: NADH oxidase activity monitored as ΔA_{340nm} vs time in a solution containing 120 μM NADH in air-saturated 100 MES at pH 5.6 and 23 °C with FprA (50 nM homodimer) added at zero time and Hrb (50 nM homodimer) added at the time indicated by the arrow. The slope of the line after the addition of Hrb corresponds to 30 μM NADH oxidized/min. The background NADH oxidase activity of Hrb in the absence of FprA under these conditions is ~1 μM NADH oxidized/min. (B) Plot of activity vs FprA concentration. Conditions: 50 nM Hrb homodimer, 200 μM NADH, and the indicated concentrations of FprA in air-saturated 50 mM phosphate, pH 7.

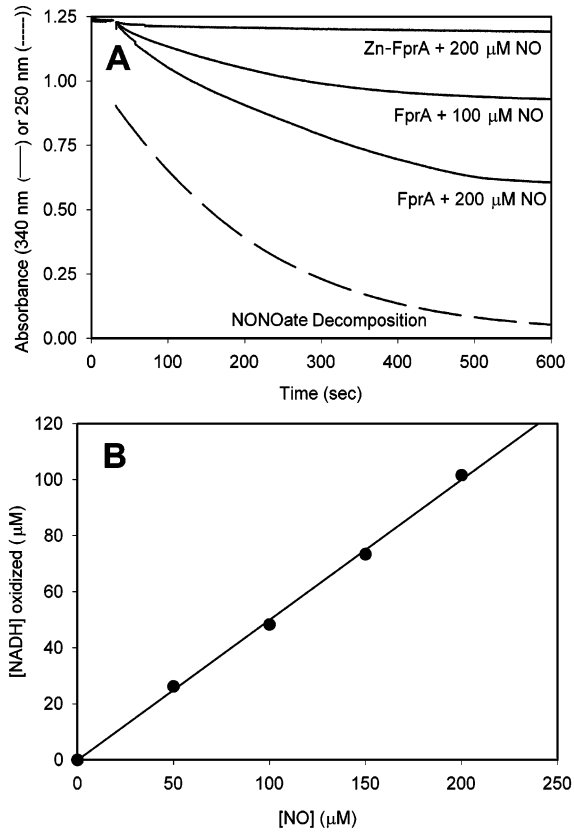

FIGURE 8: NADH:NO oxidoreductase activity of *M. thermoacetica* Hrb/FprA using DEA NONOate as the source of NO. Conditions: 0.22 μM FprA (or Zn−FprA) homodimer, 0.25 μM Hrb homodimer, 200 μM NADH in anaerobic 100 mM potassium phosphate, pH 7.0, containing 0.3 mM EDTA, 10 mM glucose + 10 units/mL glucose oxidase, and 150 units/mL catalase. (A) The rate of NADH oxidation was monitored at 340 nm and of decomposition of 133 μM DEA NONOate at 250 nm. Each mole of DEA NONOate releases 1.5 mol of NO. (B) Plot of NADH oxidized vs NO released from DEA NONOate.

NADH:FprA Oxidoreductase Activity of Hrb. The absorption spectrum of the recombinant *M. thermoacetica* FprA does not change in the presence of excess NADH or NADPH under either aerobic or anaerobic conditions, indicating that the FMN in FprA is not reduced by these pyridine nucleotides. However, as shown in Figure 6, when catalytic amounts of Hrb are added to anaerobic solutions of as-isolated FprA, addition of ≥3 reducing equivalents of NADH per FprA monomer converts the absorption spectrum of the FMN in FprA to that characteristic of the anionic semiquinone form, which has a prominent absorption feature at 390 nm and shoulder at 480 nm (*20*). The first two reducing equivalents of added NADH presumably enter the diferric site. Additions of >3 reducing equivalents of NADH do not cause further reduction of the FMN semiquinone of FprA for many hours under the conditions of Figure 6. Excess sodium dithionite, however, rapidly converts the FprA absorption spectrum to that characteristic of the two-electron-reduced FMN, i.e., the hydroquinone ($FMNH_2$). In contrast to reduction of FprA with catalytic Hrb, the inset to Figure 6 shows that the FMN semiquinone does not accumulate upon titration of an equimolar Hrb−FprA mixture with NADH. On the basis of the Hrb titration with NADH (Figure 5), it appears that, during the initial stages (i.e., the first 2−3 reducing equivalents) of this equimolar mixture titration, the $[Fe(SCys)_4]$ site of Hrb is reduced concomitantly with the FMN of FprA. Analogous experiments in which NADH was replaced with NADPH showed that Hrb has very little NADPH:FprA oxidoreductase activity.

Zn−Hrb shows no NADH:FprA oxidoreductase activity under the conditions of Figure 6, even though the FMN in Zn−Hrb *is* reduced by NADH (spectra not shown). This result, together with those in Figures 5 and 6, indicates that Hrb's NADH:FprA oxidoreductase activity involves the electron flow pathway, NADH → Hrb−FMN → Hrb−$[Fe(SCys)_4]$ → FprA, and that the $[Fe(SCys)_4]$ site in Hrb is the proximal electron donor to the FMN and/or diiron site of FprA.

NADH:Dioxygen Oxidoreductase Activity of Hrb/FprA. Dioxygen reductase activity of FprA homologues from other bacteria has been reported (*14*, *24*, *37*). Figure 7 shows that the recombinant *M. thermoacetica* FprA is also an active dioxygen reductase, but only when combined with Hrb. Similarly, Hrb has only a small background NADH oxidase activity in the absence of FprA (cf. legend to Figure 7). Analyses of the plots in Figure 7 gave $K_m = 2$ μM (monomer basis) for Hrb during its NADH:FprA oxidoreductase activ-

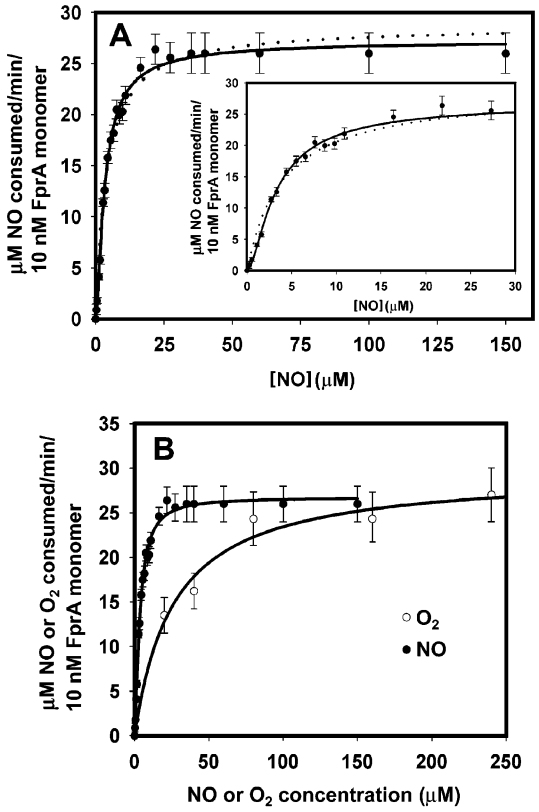

FIGURE 9: NO concentration dependence of NADH:NO reductase activity of Hrb/FprA (panel A) and comparisons of NO and O_2 concentration dependences of the respective NADH:NO reductase and NADH:O_2 reductase activities of Hrb/FprA (panel B) at saturating Hrb and NADH. Both O_2 reductase and anaerobic NO reductase assay solutions contained 5 μM Hrb homodimer, 5 nM FprA homodimer, and 200 μM NADH in 50 mM phosphate, pH 7. Data points/error bars represent the averages/ranges of five determinations. (A) Rates of NO consumption were measured using an NO electrode, as described in Materials and Methods. The curves represent least-squares fits of either the Michaelis−Menten equation (dotted trace) or eq 1 listed in the text (solid trace) to the data. Parameters for both fits are listed in the text. (B) NO reductase data (filled circles) and the solid trace through these data are the same as plotted in panel A. O_2 consumption rates (open circles) are plotted as one-half the NADH consumption rates (measured at 340 nm). The reactions were initiated by additions of O_2-saturated buffer to previously anaerobic assay solutions, and the data represent the resulting initial O_2 concentrations. The solid trace through the open circles represents a fit of the Michaelis−Menten equation to the data using parameters listed in the text.

ity. Using an oxygen electrode, the mole ratio of NADH oxidized:O_2 reduced under the conditions of Figure 7 was determined to be ~2:1 and to be unaffected by the presence of catalase; i.e., Hrb/FprA catalyzes the four-electron reduction of dioxygen to water by NADH, as has been verified for other FprAs. The K_m for O_2 is discussed below when comparing NO reductase activity. The Zn−FprA, when substituted for FprA, showed no dioxygen reductase activity above background under the conditions of Figure 7, consistent with participation of the diiron site in this activity. The data in Figure 7 were obtained from initial rates. During these assays a gradual loss of the dioxygen reductase activity of FprA was noted, similar to that observed in the kinetic traces previously reported for *E. coli* FlRd (*24*). For the *M. thermoacetica* FprA at least, this loss of O_2 reductase activity was irreversible.

NADH:NO Oxidoreductase Activity of Hrb/FprA. The fact that *M. thermoacetica* is a strict anaerobe and can use nitrate as electron acceptor, together with the observation that *E. coli* FlRd, an FprA homologue, showed anaerobic NO consumption activity, prompted us to examine this latter activity for *M. thermoacetica* Hrb/FprA. Figure 8A shows that the Hrb/FprA combination does indeed have NADH:NO oxidoreductase activity using DEA NONOate as the source of NO and that no such activity is observed when Zn−FprA is substituted for FprA. The parallel progression curves for NADH consumption and decomposition of the NONOate show that the rate-determining step under these conditions is release of NO from the NONOate. Figure 8A also shows that the total amount of NADH oxidized is proportional to the total amount of NO released by the decomposition of DEA NONOate. A plot of these and additional such data in Figure 8B gives a stoichiometry of 1 mol of NADH oxidized:2 mol of NO released, consistent with reduction of NO to N_2O. Omission of either FprA or Hrb from the assay mixture resulted in no consumption of NADH above background (similar to that shown in Figure 8 with Zn−FprA). Successive additions of aliquots of saturated aqueous NO solutions in place of DEA NONOate to anaerobic assay mixtures similar to those described in Figure 8 also yielded ~1:2 mol/mol NADH oxidized:NO added (cf. Figure 4S in Supporting Information). The NO-dependent NADH consumption activity of FprA/Hrb showed no diminution in either rate or extent, even after as many as 12 successive 5 μM injections of NO over the course of 30 min.

Figure 9A plots the NADH:NO reductase activities of FprA/Hrb at saturating Hrb and NADH, and the dotted curve is a fit of the Michaelis−Menten equation to the data (with parameters listed below). A significantly improved fit, especially at the lowest and highest NO concentrations, was obtained by adopting a kinetic scheme (Scheme 1) originally proposed for bacterial respiratory NORs that contain a binuclear heme−non-heme iron active site (*38*, *39*). According to this scheme, at saturating levels of NADH and Hrb, reduction of two NO's to N_2O occurs at a single reduced FprA active site (E_{red}).

Scheme 1

$$E_{red} + NO \overset{K_1}{\rightleftharpoons} E_{red}{-}NO$$

$$E_{red}{-}NO + NO \overset{K_2}{\rightleftharpoons} E_{red}{-}(NO)_2$$

$$E_{red}{-}(NO)_2 \xrightarrow{k_{cat}} E_{ox} + N_2O$$

The rate law applying to Scheme 1 is (*38*, *39*)

$$v = (V_{max}[NO]^2)/(K_1 + K_2[NO] + [NO]^2) \qquad (1)$$

where v is the initial velocity. Fits of eq 1 to the data plotted in Figure 9A yielded the solid curve with parameters $V_{max} = 27.3 \pm 0.4$ μM/min, corresponding to $k_{cat} = 46$ s^{-1} on a monomer, i.e., active site basis, $K_1 = 5.1 \pm 1.0$ μM, and $K_2 = 2.1 \pm 0.3$ μM. Unlike the respiratory NORs, no evidence for inhibition of FprA's NO reductase activity by NO was apparent at the highest concentrations of NO used in this work. Mechanisms consistent with Scheme 1 have been

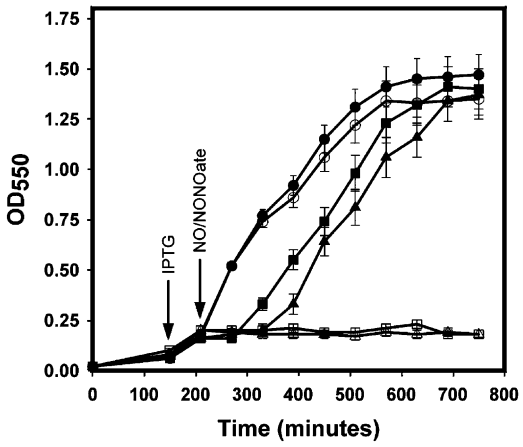

FIGURE 10: Restoration of anaerobic growth of *E. coli* AG300 in the presence of added NO by expression of plasmid-borne *M. thermoacetica fprA*. Cultures were grown in anaerobic minimal medium at 37 °C as described in Materials and Methods. Key: filled symbols, strain AG300[pFprA-pCYB1]; open symbols, control strain AG300[pCYB1]; circles, no NO added; squares, NO added to an initial concentration of 7 μM; triangles, DEA NONOate added to an initial concentration of 5 μM. IPTG and NO/DEA NONOate were added at the times following inoculation indicated by the arrows. Each data point is the average of at least four independent growth experiments.

proposed for *E. coli* FlRd (*21*), although the kinetics were not analyzed in this fashion (*25*). The similar values of K_1 and K_2 suggest that, if Scheme 1 is operative in FprA, then the bindings of the two NO's, presumably one to each iron of the diiron site, are largely independent of each other.

Plots of the NADH:NO and NADH:O_2 reductase activities as a function of NO and O_2 concentrations, respectively, are shown in Figure 9B. Fits of these data to the Michaelis−Menten equation yielded the kinetic parameters K_m, 4 μM for NO, 26 μM for O_2; k_{cat}, 50 s^{-1} for O_2, 48 s^{-1} for NO (on an FprA monomer basis); and k_{cat}/K_m, 0.19 × 10^7 s^{-1} M^{-1} for O_2, 1.2 × 10^7 s^{-1} M^{-1} for NO. As can be clearly seen from these values and the plots in Figure 9B, the recombinant *M. thermoacetica* FprA/Hrb is a more efficient NO than O_2 reductase by virtue of its lower K_m for NO.

Complementation by FprA of the E. coli ΔFlRd Strain against NO Toxicity. The *E. coli* AG300 strain contains a disrupted FlRd gene, *norV*. This strain was shown to be incapable of anaerobic growth in minimal media containing low micromolar levels of added NO, whereas the parental strain under the same conditions showed little or no growth impairment (*21*). As shown in Figure 10, IPTG-induced expression of the plasmid-borne *M. thermoacetica fprA* in strain AG300[pFprA-pCYB1] restored the anaerobic growth phenotype of cultures exposed to exogenous NO added either directly or from the NONOate.[4] Given the in vitro NO reductase activity of FprA, the logical inference from this growth complementation is that the level of intracellular NO is lowered due to the NO reductase activity of the heterologously expressed *M. thermoacetica* FprA. The lag phase in growth following addition of NO to the AG300[pFprA-pCYB1] cultures can be explained as the time required for induction of FprA and its lowering of the intracellular NO concentration to a tolerable level for growth. Since *M. thermoacetica* FprA by itself does not show NO consumption activity in vitro, but does show NADH:NO oxidoreductase activity when combined with Hrb, an endogenous *E. coli* enzyme most likely mimics Hrb's function as an NADH:FprA oxidoreductase. An analogous phenomenon occurred with *E. coli* FlRd. The gene adjacent to that encoding *E. coli* FlRd encodes a protein which functions as an NADH:FlRd oxidoreductase in vitro (*24*). Disruption of this FlRd reductase gene resulted in somewhat lower intracellular NO consumption activity but did not result in impaired anaerobic growth relative to wild type at micromolar levels of NO (*21*). The FlRd reductase in strain AG300 could conceivably function as electron donor to the heterologously expressed *M. thermoacetica* FprA. However, the *E. coli* FlRd reductase is not an Hrb homologue, nor does such a homologue exist in *E. coli*. The two domains of Hrb are instead reflected in separate modular fusions at the C-termini of two other FprAs, namely, the rubredoxin-like domain of *E. coli* FlRd and the FMN binding domain of a cyanobacterial FprA (*14*).

NO vs O_2 Reductase Function of FprA/Hrb. The turnover number (k_{cat}) for NADH:NO reductase activity of *M. thermoacetica* FprA at saturating Hrb, 48 s^{-1}, is significantly higher than the 4 ± 2 s^{-1} reported for FlRd saturated with its reductase [corrected to a monomer basis from the 15 ± 7 s^{-1} value (*25*) for the reportedly tetrameric FlRd (*18*, *24*)], whereas the K_m for NO was reported to be <1 μM for FlRd (*25*) compared to 4 μM determined in this work for *M. thermoacetica* FprA.

Given the association of *M. thermoacetica fprA* and *hrb* with genes encoding oxidative stress protection proteins (*12*) and the anaerobic growth requirement of *M. thermoacetica*, an oxidative or nitrosative stress protection function seems more likely than a direct respiratory role for the respective O_2 or NO reductase activities of FprA/Hrb. Arguments in favor of an NO over an O_2 reductase function for *M. thermoacetica* FprA include its approximately 6-fold higher catalytic efficiency (k_{cat}/K_m) for NO vs O_2, its protection of a FlRd-deficient *E. coli* strain against the toxicity of micromolar levels of added NO (which notably occurred even without its presumed native electron donor, Hrb), and its progressive, irreversible inactivation during O_2 reductase turnover but retention of activity during NO reductase turnover. It is noteworthy that, under the growth conditions of Figure 10, even submicromolar steady-state concentrations of exogenous NO are toxic to the AG300 *E. coli* strain (*21*). The *M. thermoacetica* FprA, when heterologously expressed in this strain, was, thus, apparently able to function effectively at 37 °C at NO concentrations significantly below the K_m determined for the isolated enzyme at 23 °C.

While *M. thermoacetica* was reported to grow in liquid culture under low initial percentages of O_2, it failed to grow when the initial headspace O_2 was increased to 2.0% (*11*), which corresponds to a dissolved O_2 concentration that is approximately the same as Hrb/FprA's K_m for O_2 (26 μM) determined in this work. These observations further argue against an effective O_2-scavenging function for FprA. *M. thermoacetica* could be exposed to NO as a consequence of its preference for nitrate as electron acceptor (*5*), and a nitrate reductase activity has been detected in cell extracts (*7*). Hrb/FprA shows no nitrate- or nitrite-dependent NADH con-

[4] IPTG addition did not affect the growth rates in the absence of NO. If IPTG was not added, neither AG300[pFprA-pCYB1] nor the control strain, AG300[pCYB1], grew anaerobically in the presence of NO added to the levels listed in the legend to Figure 10.

sumption activity (R. Silaghi-Dumitrescu, E. D. Coulter, and D. M. Kurtz, Jr., unpublished results). Alternatively, *M. thermoacetica* could be exposed to NO in its natural growth environment, presumed to be the mammalian intestine (*40*). We are unaware of any published studies investigating the tolerance of *M. thermoacetica* to exogenous NO. However, we have found that *M. thermoacetica* was able to grow anaerobically at 58 °C following a short lag phase upon addition of low micromolar levels of NO to a growth medium lacking reducing agents and supplied with CO_2 as electron acceptor and methanol as electron donor (A. Das, L. Ljungdahl, and D. M. Kurtz, Jr., unpublished results). Studies in progress in our laboratory, both in vivo and in vitro, are aimed at delineating the role of FprA/Hrb in nitrosative stress protection in *M. thermoacetica* and the mechanism of NO reduction by this novel combination of non-heme iron proteins.

ACKNOWLEDGMENT

We thank Richard Conover for technical assistance with EPR spectra. The Chemistry Department of Babesh-Bolyai University, Cluj-Napoca, Romania, is thanked for a leave of absence to R.S.-D.

SUPPORTING INFORMATION AVAILABLE

Description of the spectroelectrochemical titration procedure and Nernst plots, EPR spectrum of Hrb, and NADH consumption catalyzed by FprA/Hrb titrated with NO. This material is available free of charge via the Internet at http://pubs.acs.org.

REFERENCES

1. Collins, M. D., Lawson, P. A., Willems, A., Cordoba, J. J., Fernandez-Garayzabal, J., Garcia, P., Cai, J., Hippe, H., and Farrow, J. A. (1994) *Int. J. Syst. Bacteriol. 44*, 812−826.
2. Das, A., and Ljungdahl, L. G. (2000) in *Encyclopedia of Microbiology* (Lederberg, J., Ed.) pp 18−27, Academic Press, San Diego, CA.
3. Drake, H. L. (1994) in *Acetogenesis* (Drake, H. L., Ed.) pp 3−49, Chapman & Hall, New York.
4. Wood, H. G., and Ljungdahl, L. G. (1991) in *Variations of autotrophic life* (Shively, J. M., and Barton, L. L., Eds.) pp 201−250, Academic Press, New York.
5. Seifritz, C., Daniel, S. L., Gossner, A., and Drake, H. L. (1993) *J. Bacteriol. 175*, 8008−8013.
6. Frostl, J. M., Seifritz, C., and Drake, H. L. (1996) *J. Bacteriol. 178*, 4597−4603.
7. Arendsen, A. F., Soliman, M. Q., and Ragsdale, S. W. (1999) *J. Bacteriol. 181*, 1489−1495.
8. Poock, S. R., Leach, E. R., Moir, J. W., Cole, J. A., and Richardson, D. J. (2002) *J. Biol. Chem. 277*, 23664−23669.
9. Anjum, M. F., Stevanin, T. M., Read, R. C., and Moir, J. W. (2002) *J. Bacteriol. 184*, 2987−2893.
10. Frey, A. D., Farres, J., Bollinger, C. J., and Kallio, P. T. (2002) *Appl. Environ. Microbiol. 68*, 4835−4840.
11. Karnholz, A., Küsel, K., Gossner, A., Schramm, A., and Drake, H. L. (2002) *Appl. Environ. Microbiol. 68*, 1005−1009.
12. Das, A., Coulter, E. D., Kurtz, D. M., and Ljungdahl, L. G. (2001) *J. Bacteriol. 183*, 1560−1567.
13. Vadas, A., Monbouquette, H. G., Johnson, E., and Schroder, I. (1999) *J. Biol. Chem. 274*, 36715−36721.
14. Vicente, J. B., Gomes, C. M., Wasserfallen, A., and Teixeira, M. (2002) *Biochem. Biophys. Res. Commun. 294*, 82−87.
15. Chen, L., Liu, M. Y., LeGall, J., Fareleira, P., Santos, H., and Xavier, A. V. (1993) *Biochem. Biophys. Res. Commun. 193*, 100−105.
16. Gomes, C. M., Silva, G., Oliveira, S., LeGall, J., Liu, M. Y., Xavier, A. V., Rodrigues-Pousada, C., and Teixeira, M. (1997) *J. Biol. Chem. 272*, 22502−22508.
17. Frazão, C., Silva, G., Gomes, C. M., Matias, P., Coelho, R., Sieker, L., Macedo, S., Liu, M. Y., Oliveira, S., Teixeira, M., Xavier, A. V., Rodrigues-Pousada, C., Carrondo, M. A., and Le Gall, J. (2000) *Nat. Struct. Biol. 7*, 1041−1045.
18. Wasserfallen, A., Ragettli, S., Jouanneau, Y., and Leisinger, T. (1998) *Eur. J. Biochem. 254*, 325−332.
19. Gomes, C. M., Frazao, C., Xavier, A. V., Legall, J., and Teixeira, M. (2002) *Protein Sci. 11*, 707−712.
20. Jouanneau, Y., Meyer, C., Asso, M., Guigliarelli, B., and Willison, J. C. (2000) *Eur. J. Biochem. 267*, 780−787.
21. Gardner, A. M., Helmick, R. A., and Gardner, P. R. (2002) *J. Biol. Chem. 277*, 8172−8177.
22. Gardner, A. M., and Gardner, P. R. (2002) *J. Biol. Chem. 277*, 8166−8171.
23. Hutchings, M. I., Mandhana, N., and Spiro, S. (2002) *J. Bacteriol. 184*, 4640−4643.
24. Gomes, C. M., Vicente, J. B., Wasserfallen, A., and Teixeira, M. (2000) *Biochemistry 39*, 16230−16237.
25. Gomes, C. M., Giuffre, A., Forte, E., Vicente, J. B., Saraiva, L. M., Brunori, M., and Teixeira, M. (2002) *J. Biol. Chem. 277*, 25273−25276.
26. Das, A., Hugenholtz, J., Van Halbeek, H., and Ljungdahl, L. G. (1989) *J. Bacteriol. 171*, 5823−5829.
27. Sambrook, J., Fritsch, E. F., and Maniatis, T. (1990) *Molecular cloning: a laboratory manual.*, 2nd ed., Cold Spring Harbor Laboratory Press, Cold Spring Harbor, NY.
28. Schagger, H., and von Jagow, G. (1987) *Anal. Biochem. 166*, 368−379.
29. Xiong, J., Kurtz, D. M., Jr., Ai, J., and Sanders-Loehr, J. (2000) *Biochemistry 39*, 5117−5125.
30. Harlow, E., and Lane, D. (1988) *Antibodies: a laboratory manual*, Cold Spring Harbor Laboratory Press, Cold Spring Harbor, NY.
31. Eby, D. M., Beharry, Z. M., Coulter, E. D., Kurtz, D. M., Jr., and Neidle, E. L. (2001) *J. Bacteriol. 183*, 109−118.
32. Solomon, E. I., Brunold, T. C., Davis, M. I., Kemsley, J. N., Lee, S.-K., Lehnert, N., Neese, F., Skulan, A. J., Yang, Y.-S., and Zhou, J. (2000) *Chem. Rev. 100*, 235−349.
33. Chiu, H.-J., Johnson, E., Schroder, I., and Rees, D. C. (2001) *Structure 9*, 311−319.
34. Eidsness, M. K., Burden, A. E., Richie, K. A., Kurtz, D. M., Jr., Scott, R. A., Smith, E. T., Ichiye, T., Beard, B., Min, T., and Kang, C. (1999) *Biochemistry 38*, 14803−14809.
35. Eidsness, M. K., Burden, A. E., Richie, K. A., Kurtz, D. M., Jr., Scott, R. A., Smith, E. T., Ichiye, T., Beard, B., Min, T., and Kang, C. (2000) *Biochemistry 39*, 626.
36. Zeng, Q., Smith, E. T., Kurtz, D. M., Jr., and Scott, R. A. (1996) *Inorg. Chim. Acta 242*, 245−251.
37. Chen, L., Liu, M. Y., Legall, J., Fareleira, P., Santos, H., and Xavier, A. V. (1993) *Eur. J. Biochem. 216*, 443−448.
38. Girsch, P., and de Vries, S. (1997) *Biochim. Biophys. Acta 1318*, 202−216.
39. Koutny, M., and Kucera, I. (1999) *Biochem. Biophys. Res. Commun. 262*, 562−564.
40. Breznak, J. A., and Kane, M. D. (1990) *FEMS Microbiol. Rev. 7*, 309−313.

BI027253K